Supplementary Information: Formation and stability of transverse and longitudinal sand dunes

E. Reffet, S. Courrech du Pont, P. Hersen, and S. Douady

Laboratoire MSC, Université Paris-Diderot, CNRS , France. and LESIA, Observatoire de Paris, CNRS, France.

Contents

I. EXPERIMENTAL DETAILS

A. Experimental setup

Here, we describe in detail the experimental setup used in this study (Fig. 1). A plate (90 cm wide and 1 m long), on which we put sand, is immersed in a 2 m long and 1 m wide water tank. Bleach is added to the water to prevent bacteria and algae proliferation. To reproduce the effect of a mono-directional current, the plate is quickly translated by a motorized engine from one end to the other of the water tank. The plate gently stops and gets back to its initial position at a much lower velocity to prevent grain motion. This asymmetric motion, a stroke, simulates, in the frame of the moving plate, a mono-directional wind blowing on the sand bed put on the plate. The center of the plate is a disk which can be rotated. Rotating the dune field developing on its surface changes the wind direction can be changed by . The slow rotation of the disk is driven by a computer-controlled step-motor. Mechanical perturbations, such as stick-slip effects, lead to an angle variation of less than 1° but no angular drift. The disk has a diameter of 70 cm so that the region of interest is much larger than the characteristic scale (centimeters) of the observed patterns. By periodically changing the orientation by an angle $\pm\theta$, this setup reproduces the effect of a bimodal wind regime on a sand bed. We chose to modify the wind direction every 2 strokes to simulate a symmetric and periodic bimodal wind regime. 2 strokes is the typical amount of motion needed to adapt partially the shape of the structures to the actual wind. Increasing, in a reasonable range, the number of strokes between two rotations does not affect significantly the results (see I.D). A typical experiment counts several hundreds of periods, 1 period is equal to 2 x 2 strokes (2 strokes per direction).

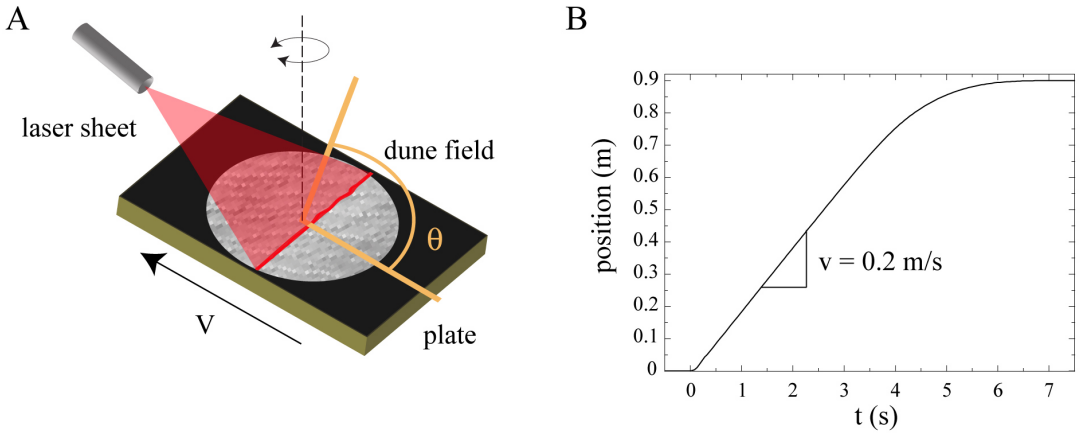

FIG. 1 **Experimental setup. A**. Sketch of the experimental setup, showing the plate, the rotatable central disk on which a dune field develops and the laser diode for $3D$ reconstruction of the sand bed profile. **B**. Typical motion of the plate during the fast forward motion (stroke).

Though subaqueous dunes can also be reproduced with natural sand, we use roughly spherical and size-calibrated ceramic beads (from 65 to 120 μm). For a typical experiment we used 600 g of beads spread on the central disk, forming a sand layer about 1 mm high. A camera, moving with the plate, records pictures of the sand bed from the top. The whole water tank is isolated from the exterior light to keep constant lighting conditions - and therefore picture quality - during the whole experiment. A rod of LED is used to produce a raking light. A laser beam is also used in order to determine the height profiles of the sand beds. Finally, the experiment is fully automated through computer control. This experimental approach has been successfully used to study barchans in the lab (1), to evidence the process of barchan collisions (2) and to discuss the relation between their shape and velocity (3). This experimental setup allows a complete control of wind directions with time and therefore to perform quantitative experiments of complex wind regimes.

The following describes in particular (i) the importance of lighting orientation to analyze the sand bed morphology (I.B), (ii) the subsequent need to have a quantitative measurement of the sand bed profile and its experimental implementation (I.C) and finally (iii) the influence of the number of strokes between two wind rotations (I.D).

B. Influence of light orientation

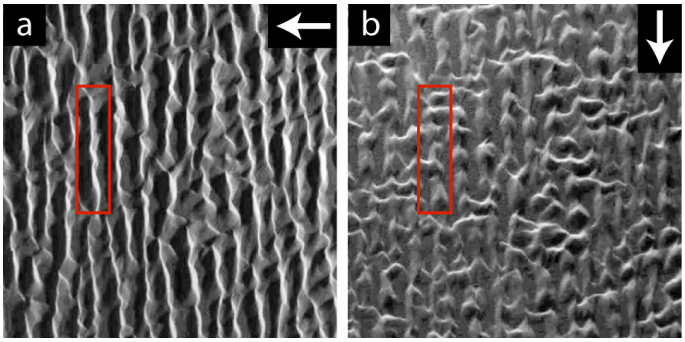

FIG. 2 **Importance of light orientation**. We compare the pictures taken with two different positions of the light source relatively to the sand bed. The same area is shown with : **(a)** light coming from the right and **(b)** light coming from the top as indicated by the arrows. While longitudinal structures are favored and the sand bed seems quite regular in **(a)**, transverse features are enhanced and the sand bed looks much more irregular in **(b)**. This shows how important it is to have a quantitative method to measure the sand bed profile for our study rather than only relying on top-view pictures.

In order to get high quality pictures, we use a raking light made with a line of white LEDs. This is ideal to enhance the topography of the sand bed. The slopes facing the light appear bright and the ones facing the opposite side are shadowed. However, since this study deals with structures with a specific orientation (parallel or perpendicular to the average wind direction), we had to be careful not to favor one orientation compared to the other while imaging the evolution of the sand bed. To do so, we use the rotation ability of the plate to take two pictures with perpendicular light orientations of the same bed-form. As illustrated in Fig.2, patterns may look significantly different depending on the light orientation. The example of Fig.2 shows the sand bed structure near the transition from transverse to longitudinal dunes. Both light orientations give information and are complementary to analyze the morphology of the sand bed. This is a striking example that needs to be remembered when analyzing pictures of sand beds. This is why we developed a quantitative $3D$ measurement of the sand bed profile using a laser diode. This method is described in the next section (I.C).

C. Three dimensional reconstruction

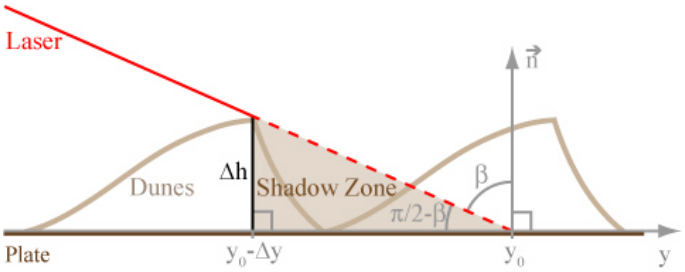

FIG. 3 **Principle of a laser scan**. Comparing the intersection position of the laser sheet with the sand bed and the plate without sand enables to measure the height using the relation $\Delta h = \Delta y * tan(\pi/2 - \beta)$. Where Δy is the shift (from the position of reference y_0) of the intersection of the laser with the sand bed due to the relief, β the incidence angle of the laser and Δh the height to be determined. We can see that there is a shadow zone where no height value can be measured on the lee side of any relief.

Given the importance of light orientation, we had to get a three dimensional reconstruction of the sand bed at specific time points to quantitatively study the respective existence domain of transverse and longitudinal dunes. We used the classic method of the deformation of a laser sheet by the sand bed surface (4). A laser beam with a prism is immersed in the water tank - to avoid optical geometric deformation at the air/water interface - and creates an intense laser sheet. It intersects the sand bed profile with a given incidence angle and draws a line if the sand bed

is flat. If the sand bed is not flat, this line is deformed and its horizontal deformation is related to the local height of the sand bed (Fig.3). Moreover, it is possible to scan the entire dune field by moving the plate under the laser sheet while imaging the intersection line between the sand bed and the laser sheet. We typically use an incidence angle of 84° with an expected height sensibility of about $0.055\,mm$. However, there is data loss in the lee side of sand reliefs. This data loss depends on the orientation of the structures within the sand bed relatively to the laser plan. Thus, we performed 4 scans of the sand bed for 4 different orientations (every 90°) between the sand bed and the laser sheet (Fig.4). The scans are then combined by a correlation procedure. The remaining gap, due to missing data, are filled by doing a bilinear interpolation. The whole process of a $3D$ profile reconstruction can be seen on Fig.4.

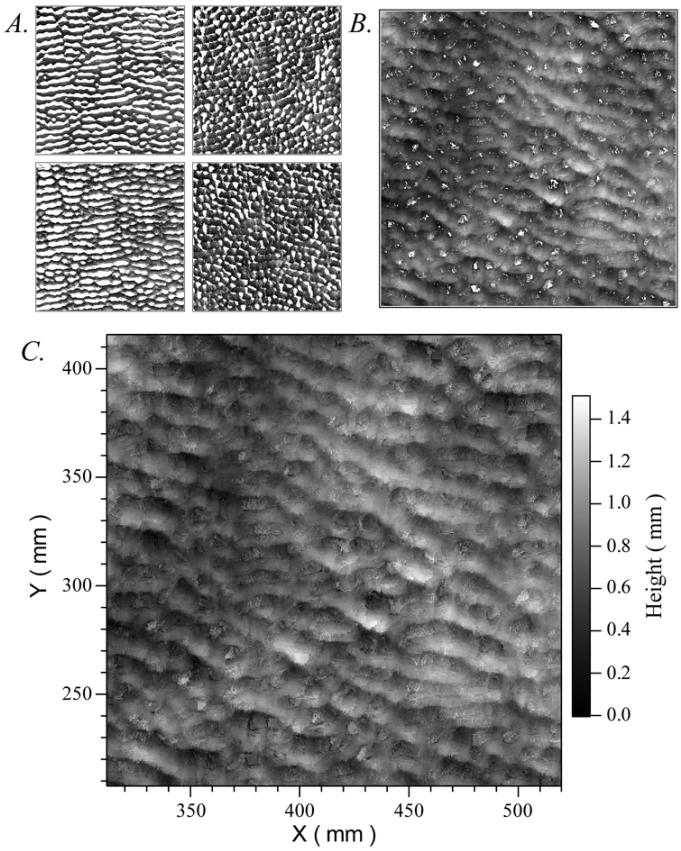

FIG. 4 **Reconstruction of the height profile of the sand bed**. **A**. Reconstruction for each orientation of the sand bed brought back to the orientation of the mean wind direction. **B**. Combination of the 4 orientations where plain white areas correspond to missing data. **C**. 3D profile completed using bilinear interpolation.

D. Influence of the number of strokes between two plate rotations

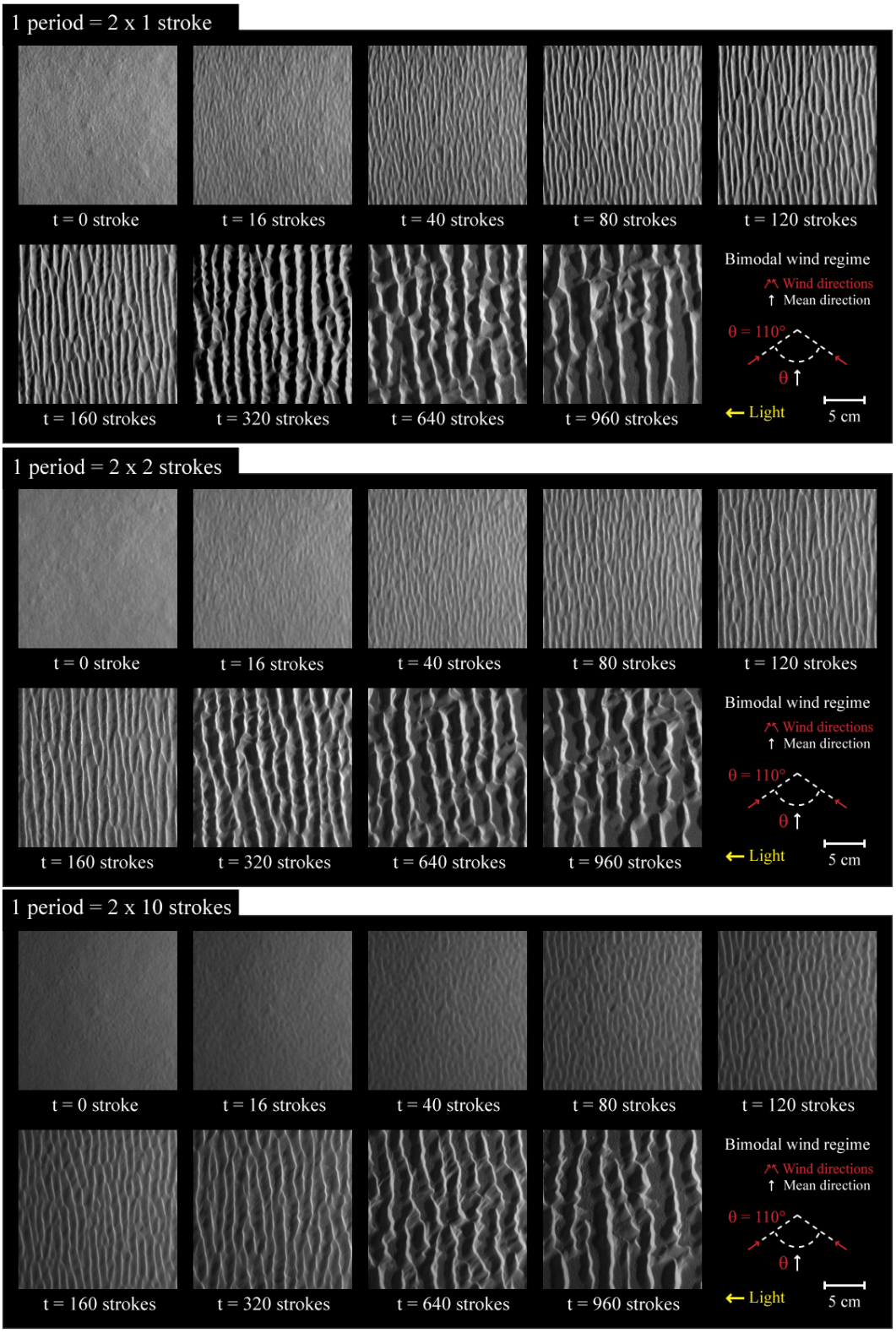

FIG. 5 **Influence of the number of strokes between two plate rotations.** The angle between the two wind directions is $\theta = 110^\circ$. All images have the same scale. The similarity between the three pattern sequences shows that the number of strokes has only a weak effect. Further experiments will be conducted to investigate precisely the influence of this parameter.

We checked that increasing the number of strokes within a period, in a relatively large range, does not affect the results of our study. In particular, transverse or longitudinal dunes still form, for the same θ value, if the number of strokes is increased from one rotation every 1 stroke to one rotation every 10 strokes. This is illustrated on Fig.5, where a set of longitudinal dunes develop for 2×1 stroke period, 2×2 stroke period and 2×10 stroke period experiments. Indeed, neither the number of strokes, nor the wind strength affect qualitatively the results as long as sand structures are big enough to integrate the bimodal wind regime. However, a complete study of the influence of this parameter on the dynamics or the details of the shape of dunes is outside the scope of this study. All experiments but these ones were done with periods of 2×2 strokes.

II. NUMERICAL MODEL

Various numerical models exist for computing the evolution of a sand bed. The model used here contains only the minimal physical ingredients to explain both the onset of sand bed instability when blown by a constant wind and the formation of three dimensional structures such as barchans. The following sections briefly describe this model. For details, see for example (5; 7) or the alternative model proposed by Hans Herrmann and collaborators (6). Note that our approach is dedicated to extract physical ingredients rather than to precisely match real geological situations. The numerical model is written in *C* language and is accessible upon request.

A. Basics of dune modeling

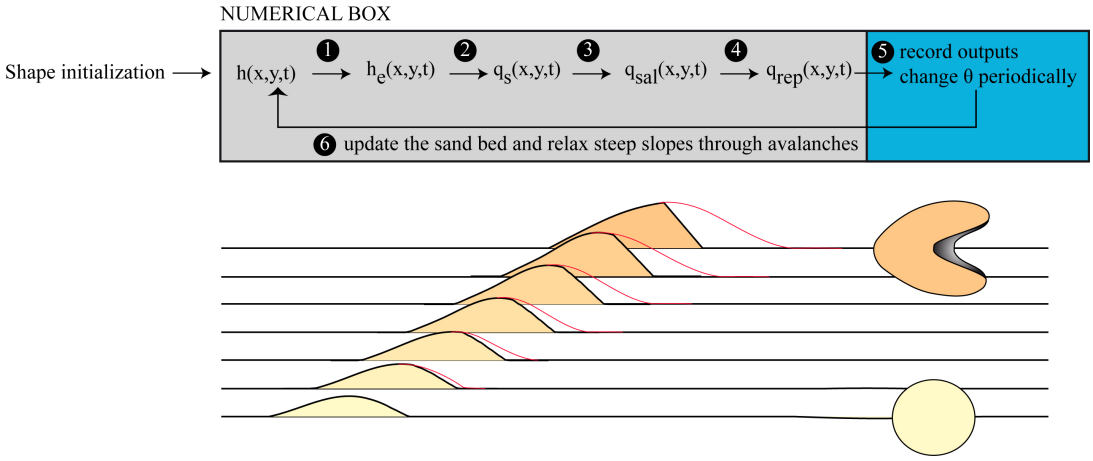

FIG. 6 **Principle of dune modeling.** 1. Compute the "envelope" of the dune to remove the discontinuity. 2. Compute the saturated sand flux (eqn.2). 3. Compute the real saltating sand flux (eqn.1). 4. Compute the reptating sand flux (eqn.3). 5. Record outputs, change physical parameters such as θ and then update the sand bed through mass conservation (6).

Let us consider a two dimensional sand bed, with a local height of sand $h = h(x, y, t)$ blown by a turbulent wind. Grains are dragged by the wind generating a sand flux. Two types of grain motion account for the sand flux : saltation and reptation (7). Saltating grains are accelerated by the wind, and move by successive rebounds on the sand bed. After each impact, they rise in the wind boundary layer and accelerate before colliding back the sand bed because of gravity. When a saltating grain impacts the sand bed, it may promote new grains to saltation and/or eject many grains of low energy which simply roll over the surface. Those are reptating grains. Let's call $q_{sal} = q_{sal}(x, y, t)$ the saltation sand flux. This sand flux is supposed to be mainly in the wind direction (6). After a characteristic length l_s, it reaches a saturated value $q_s(x, y, t)$, where no more still grains or grains in reptation can be promoted to a saltation trajectory. l_s is known to scale with the drag length, *i.e.* proportional to the size of grains times the density ratio between grains and the fluid (1; 6). For the sake of simplicity we use the following equation to relate q_{sal} and q_s :

$$\partial_x q_{sal} = \frac{q_s - q_{sal}}{l_s}\,, \tag{1}$$

The saturated value depends on the local wind speed and on the shape of the bedform. It is computed through :

$$q_s = Q(1 + A\int \frac{\partial_\xi h}{x - \xi} d\xi + B\partial_x h)\,, \tag{2}$$

where Q is a dimensional parameter and A and B are phenomenological parameters (7). This expression has been first proposed by Hans Herrmann and collaborators in a slightly different form (6). The integral term can be seen as the effect of a flat hill on the speed of the air flow - which is directly related to the saturated value of the sand flux - whereas the second term accounts for the increased erosion on positive slopes. Note that the wind is not deflected

too much by the sand bed topography because of dunes flat aspect ratio, and therefore we assume that the saturated sand flux can be computed only through x derivatives and that saturation only occurs along this axis. As stated above, saltating grains create a creeping motion of sand grains at the surface of the sand bed. The associated sand flux is proportional to the amplitude of the saltation flux and is written as :

$$\mathbf{q_{rep}} = q_{sal}(\alpha \mathbf{e_x} + \beta \nabla h), \tag{3}$$

where α and β stand respectively for the proportion of reptating grains in the wind direction and along the steepest slope. Finally, the local height of the sand bed, h, can be updated through mass conservation equation :

$$\partial_t h + \nabla(q_{rep} + q_{sal}) = 0\,, \tag{4}$$

which can be rewritten as :

$$\partial_t h + \partial_x \tilde{q} + D\nabla(\tilde{q}\nabla h) = 0\,, \tag{5}$$

where $\tilde{q}$ is the total sand flux along the wind direction (saltation and reptation, $\tilde{q} = q_{sal}(1+\alpha)$) and D is a parameter which controls the amplitude of the sand flux along the steepest slope ($D = \beta/(1+\alpha)$). The numerical model also takes into account avalanches if the local slope exceeds a threshold μ_d and the fact that erosion only happens if $h \geq 0$. Finally, the numerical model includes flow separation on the lee side of dunes : if the dune slope is somewhere steeper than a value μ_b, an idealized separation streamline is computed by fitting a third order polynomia with appropriate C^1 matching at the dune crest and at the downwind reattachment point. This point is found iteratively, so that the separation streamline is never steeper than a user-given threshold μ_b. This streamline is used to compute the saturated sand flux through fast Fourier transform algorithm. See Fig.6 for a sketch of the numerical process. This approach has been used successfully to model barchan dunes dynamics and to understand the origin of barchans shape as a tradeoff between advection and sand flux redirection through reptation (7).

B. Parameters of the numerical model

All numerical runs have been done using open boundary conditions to ensure that we do not capture marginally stable states. This is a crucial point when running simulations, since the incoming sand flux has a direct influence on the overall shape of the dune field. In our case, the input sand flux was fixed to 0 for isolated patches and bars, and only the direction of the wind was changed periodically (see Table.I). The following table lists the parameters of the numerical model and their meanings.

Parameter	range	comments
Nx,Ny	1024	Size of the grid
dx	0.2 - 1.5	Spatial resolution in units of l_s
dt	0.0001 - 0.01	Time step
E	100.0	Super-diffusion coefficient used to implement avalanches
μ_d	0.5	Threshold slope for computing avalanches
μ_b	0.25	Threshold parameter to compute separation streamline
A	9.0	Global flow parameter
B	5.0	Local flow parameter
D	0.5	Reptation parameter
q_0	0.0 - 0.1	Influx in units of saturated sand flux Q_s
BC	NA	Boundary conditions are "open"
$\theta/2$	0-90	Angle to the mean wind direction

TABLE I **Typical parameters** used in our numerical simulations. For more details about these parameters see (7). The model is scaled using two dimensional parameters : l_s, the saturation length and Q, the saturated sand flux on a flat sand bed. It allows us to define a typical timescale $\tau = l_s^2/Q$.

III. SIMPLE STABILITY ANALYSIS

A flat sand bed blown by winds destabilizes into dunes. The amplitude of the most unstable wave length grows at a particular rate which depends on flow parameters. This growth of dune height obviously needs the transportation of grains. Thus, taking into account that for a mono-directional wind, dunes form perpendicularly to the wind direction, one can assume that, at first order, the growth rate of dune height is linear with the sand flow rate that crosses its crest perpendicularly. Let us now consider a dune as sketched on figure 7 A and B. It is periodically blown by two winds of different direction but of equal strength and during the same duration. The two wind directions are making an angle θ ranging from 0 to 180°, and the dune crest is making an angle β with the mean wind direction. β ranges from 0 to 90°. As we defined it, the non-dimensional growth rate σ (*i.e* divided by half the growth rate for a mono-directional wind regime, $\theta = 0°$) writes in function of θ and β:

$$\sigma = \sin(\beta - \theta/2) + \sin(\beta + \theta/2) \text{ when } \beta >= \theta/2, \text{ or} \tag{6}$$

$$\sigma = \sin(\theta/2 - \beta) + \sin(\beta + \theta/2) \text{ when } \beta <= \theta/2, \tag{7}$$

depending if winds blow the crest from the same side or not as shown on figure 7 A and B. Figure 7 C shows σ in function of β for various θ values.

One can see that transverse and longitudinal modes are here both attractors. Starting from a minimum value that depends on θ, the growth rate increases to its maximum values when β goes to 0 (longitudinal mode) or 90° (transverse mode). Thus, a dune making an angle β with the mean wind direction will turn into a transverse dune (perpendicular to the mean wind direction) or into a longitudinal dune (parallel to the mean wind direction) in function of the starting β value: the transverse mode when starting with $\beta >= \theta/2$ (figure 7 A, eq. 6) and the longitudinal mode when $\beta <= \theta/2$ (figure 7 B, eq. 7). When a flat sand bed is blown alternatively by two winds, crests naturally first form perpendicularly to the independent winds, which corresponds to an initial β value: $\beta = \pi/2 - \theta/2$ (circles on figure 7 C). Thus, the transverse mode emerges when $\theta < 90°$ and the longitudinal mode when $\theta > 90°$ and dunes align so that the sand flow rate perpendicular to their crest is maximum as already observed by Rubin (8). When $\theta \simeq 90°$, the two modes are attractors and a composed pattern forms.

Note that if this rough model gives the right trend, it cannot render the difference of dynamics between transverse and longitudinal dunes. Moreover, we know that a transverse dune in a longitudinal regime ($\theta \gg 90°$) or a longitudinal dune in a transverse regime ($\theta \ll 90°$) destabilizes as a flat bed would.

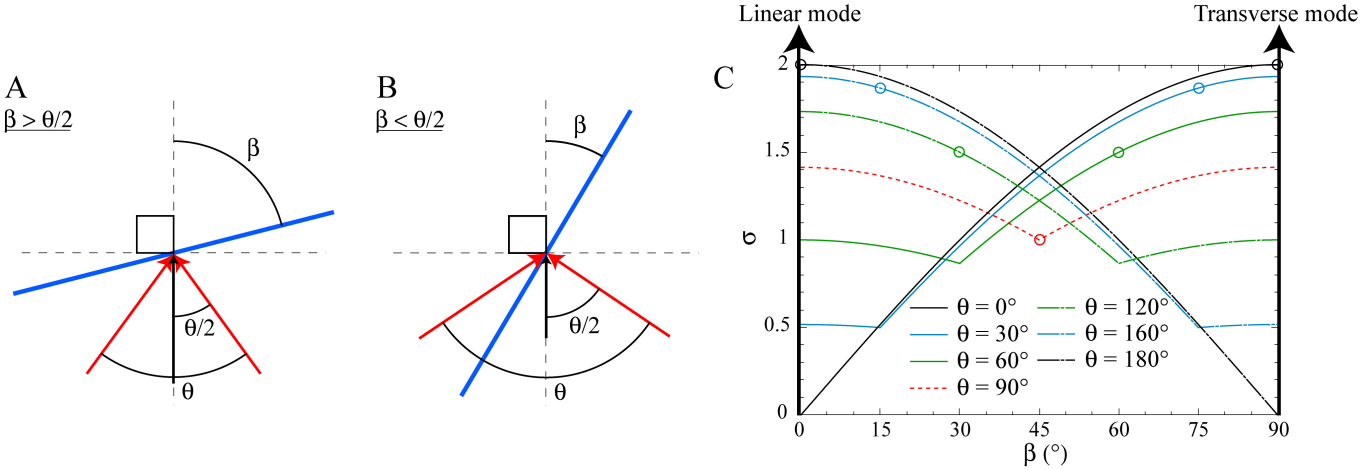

FIG. 7 **Linear analysis. A** and **B**: Sketches of a dune blown by two winds making an angle θ (red arrows). The dune crest (blue segment) makes an angle β with the mean wind (black arrow). **A**: $\beta > \theta/2$. **B**: $\beta < \theta/2$. **C**: Non-dimensional growth rate σ (as calculated with equations 6 and 7) in function of β for various θ values. circles are points where $\beta = \pi/2 - \theta/2$.

IV. SAND DUNES IN THE FIELD

A. Barchans

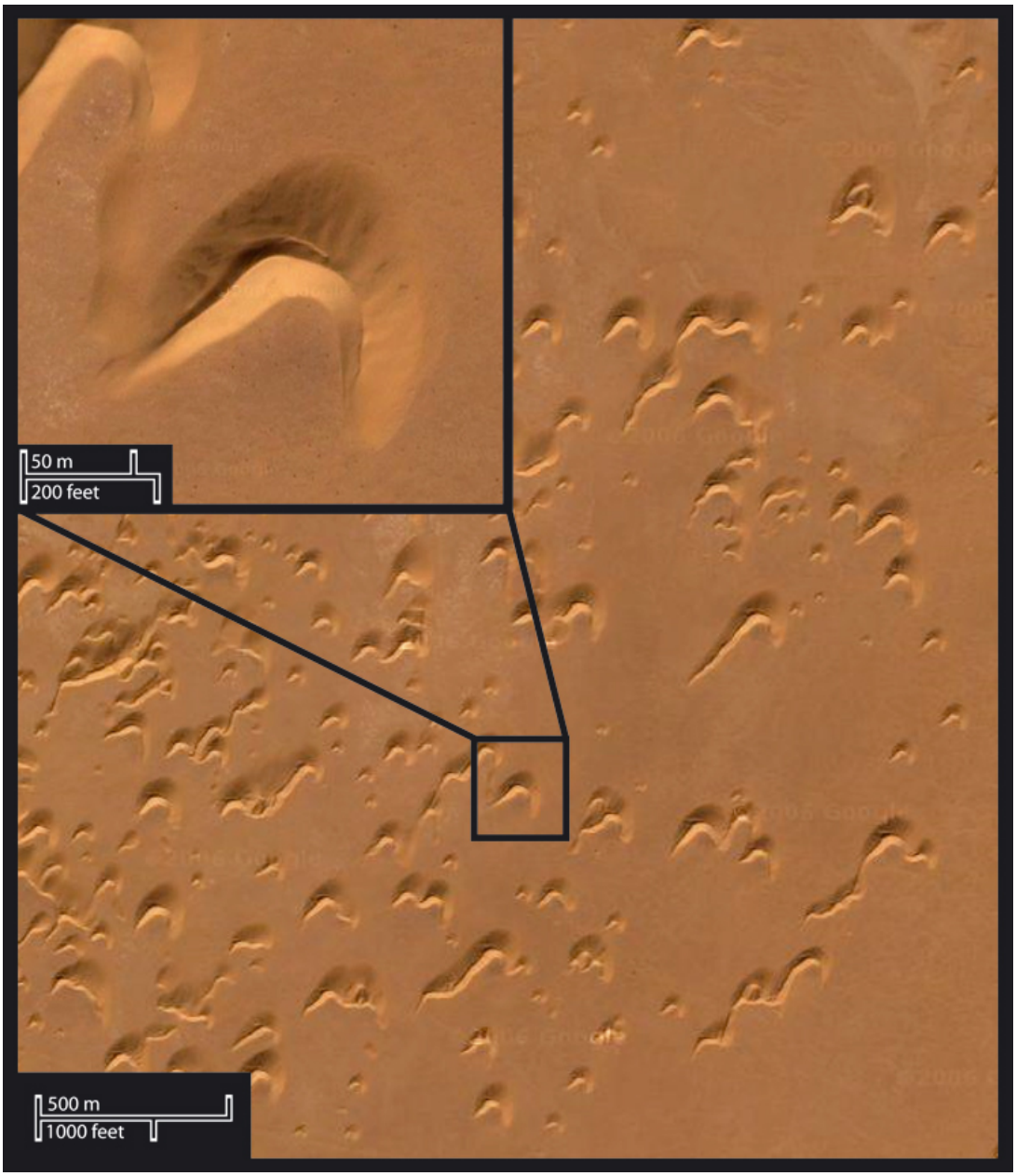

FIG. 8 **Barchan dunes.** Typical barchan dunes field, south of La'ayoune, Morocco ($26.813^\circ N$, $-13.371^\circ E$) (9).

B. Star dunes

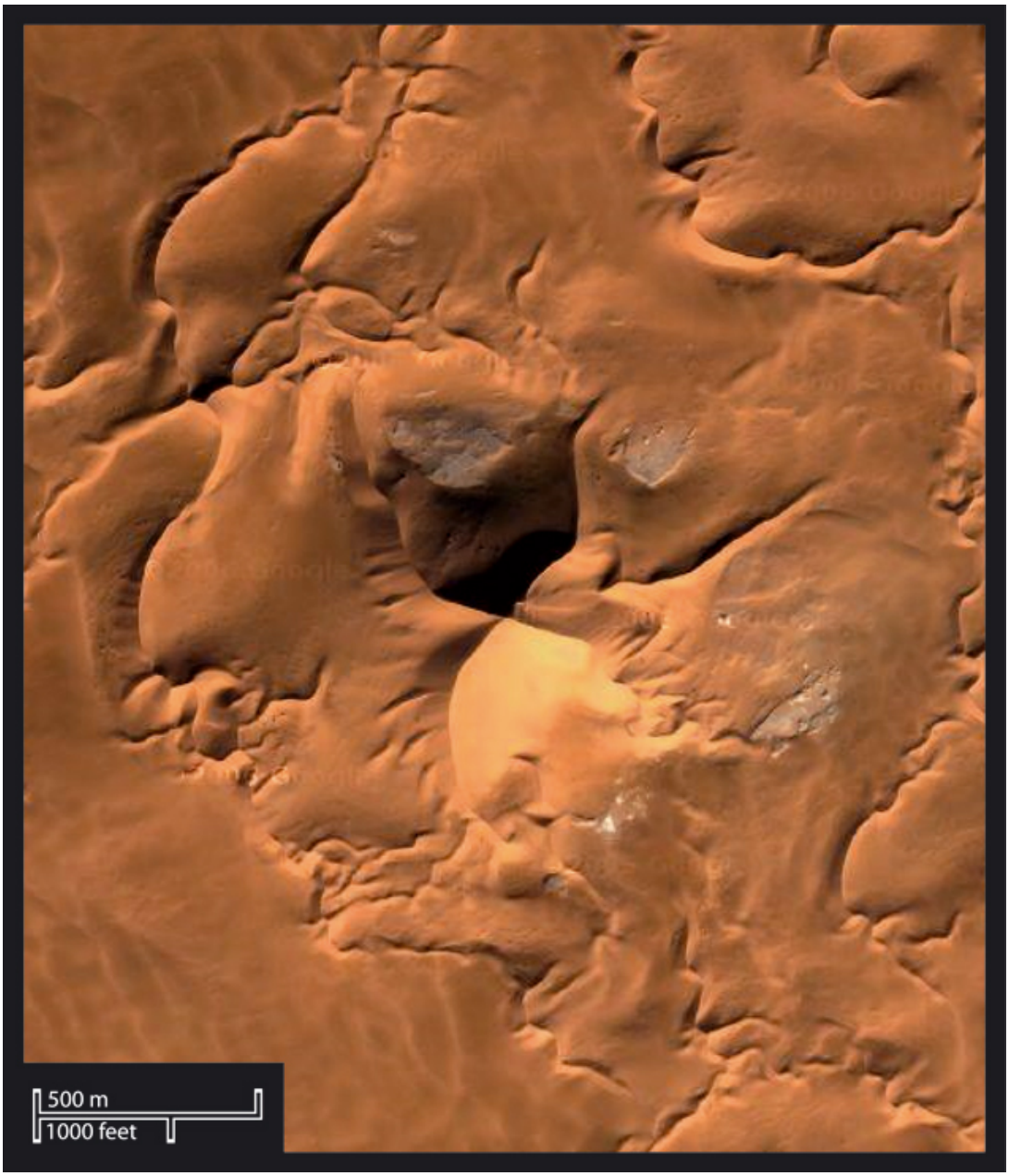

FIG. 9 **Star dunes.** Star dunes from a vast field of star dunes in the south-eastern Sahara ($30.752^\circ N$, $7.914^\circ E$) (9).

C. From barchans to longitudinal dunes

FIG. 10 **From barchans to longitudinal dunes.** Large patches of sand with a typical "chestnut" or barchan shape are transforming into long straight longitudinal dunes. This elongation matches the one obtained in our laboratory experiments and numerical simulation. Mauritania Desert ($20.964^\circ N$, $-16.813^\circ E$) (9)

D. Titan longitudinal dunes

FIG. 11 **Longitudinal dunes in Belet sand sea on Titan.** Longitudinal dunes extend on hundreds of kilometers. These mega dunes are about 100m high and $1-2\,km$ wide. They are morphologically similar to terrestrial longitudinal dunes (as the ones observed in the Namibia desert) but are likely comprised of hydrocarbons and water ice particles. Image acquired by the radar on board Cassini during $T8$ flyby. Resolution $175\,m/px$, radar illumination from the top (North).

E. Mars dunes

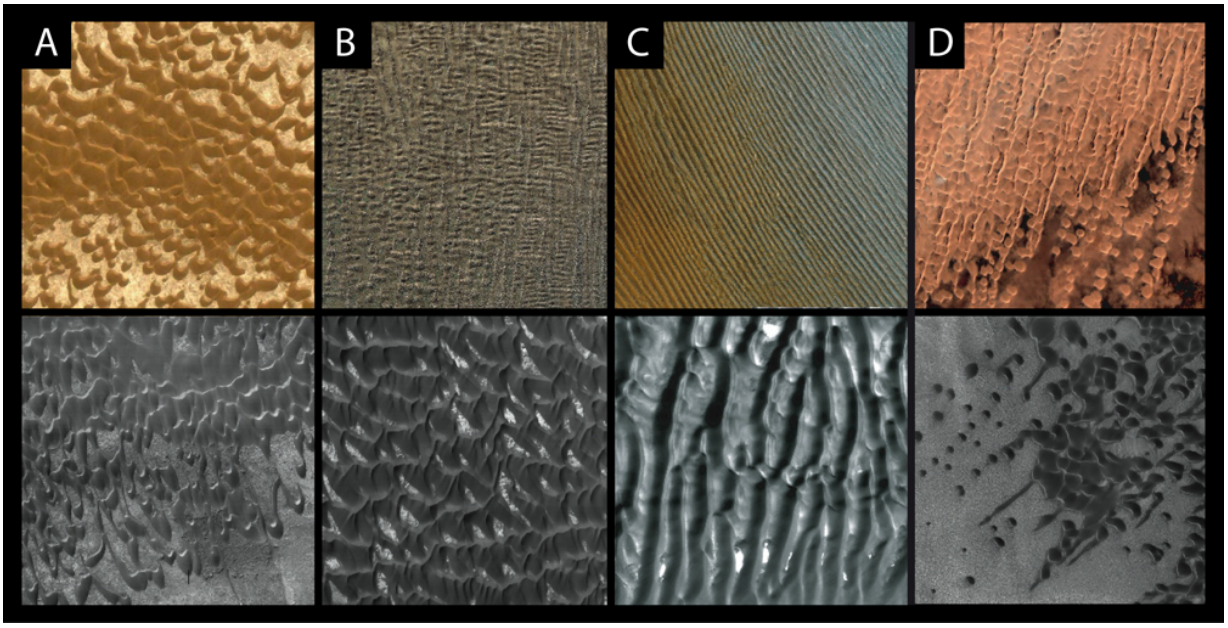

FIG. 12 **Mars dunes vs Earth dunes**. Mars also show various kinds of dunes on its surface. The first row of pictures are taken from Earth dunes (9), the second row are Mars dunes (©Nasa). **A**. Barchanoid ridges (transverse dunes). **B**. Intermediate mix state with both transverse and longitudinal structures. **C**. Longitudinal dunes. **D**. Chestnut and barchan transforming into longitudinal dunes. In the experiment, chestnut dunes form when the two blowing winds are making an angle of 90°, value at the transition between the transverse and the longitudinal mode. In the field, one can see that they are observed together with barchans and longitudinal dunes. This highlights the fact that they are transitory structures.

V. SAND DUNES IN THE LAB

A. Transverse dunes: $\theta = 33°$

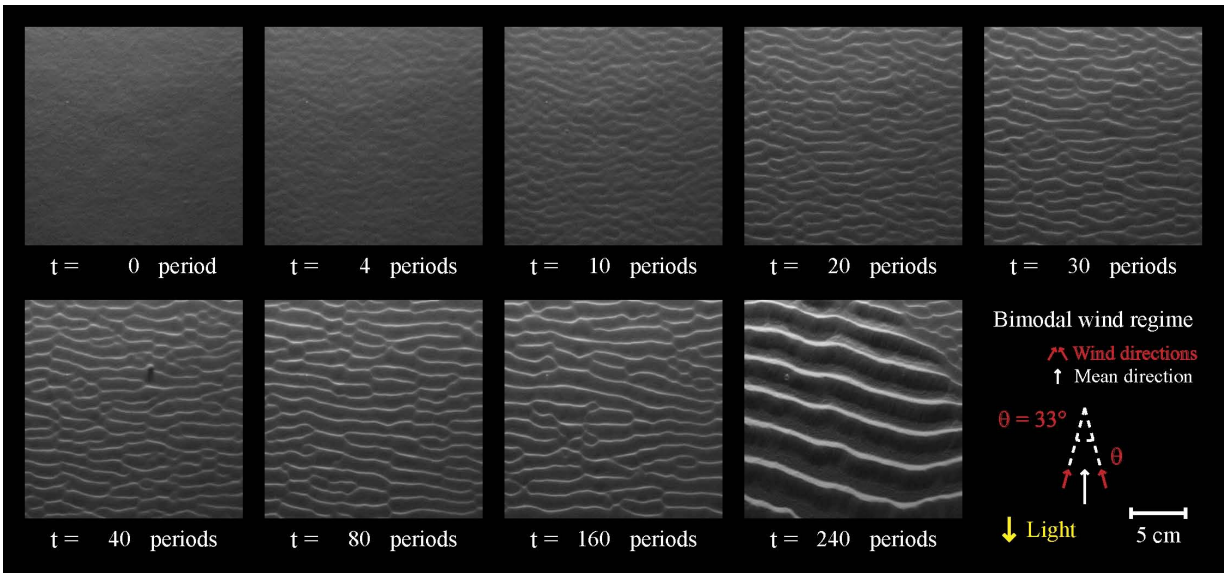

FIG. 13 **Formation of transverse sand dunes from a flat sand layer for** $\theta = 33°$. See supplementary movie *SM1* online.

B. Mixed states : $\theta = 85^\circ$

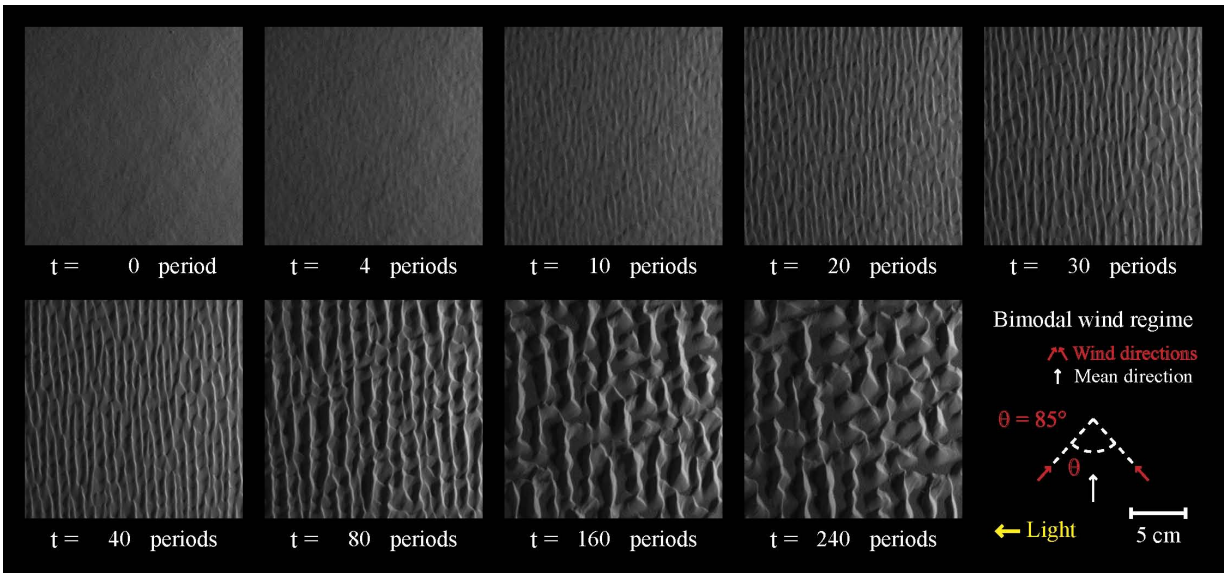

FIG. 14 **Formation of a mixed state from a flat sand layer.** The lighting enhances longitudinal structures. See supplementary movie *SM2* online.

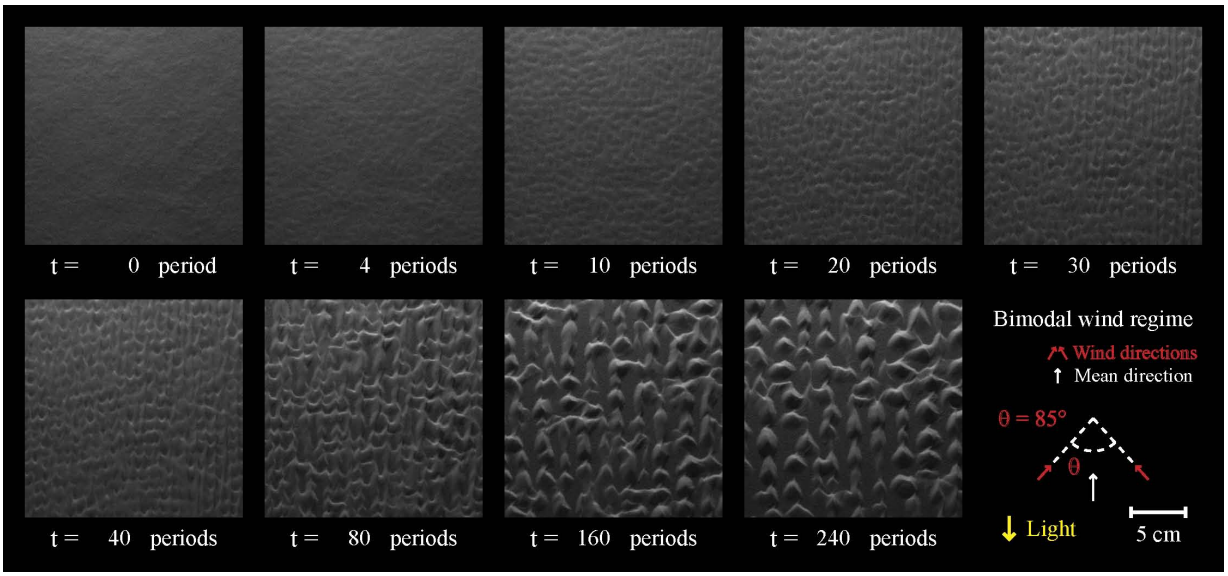

FIG. 15 **Formation of a mixed state from a flat sand layer.** The lighting enhances transverse structures. See supplementary movie *SM3* online.

C. Longitudinal dunes : $\theta = 135°$

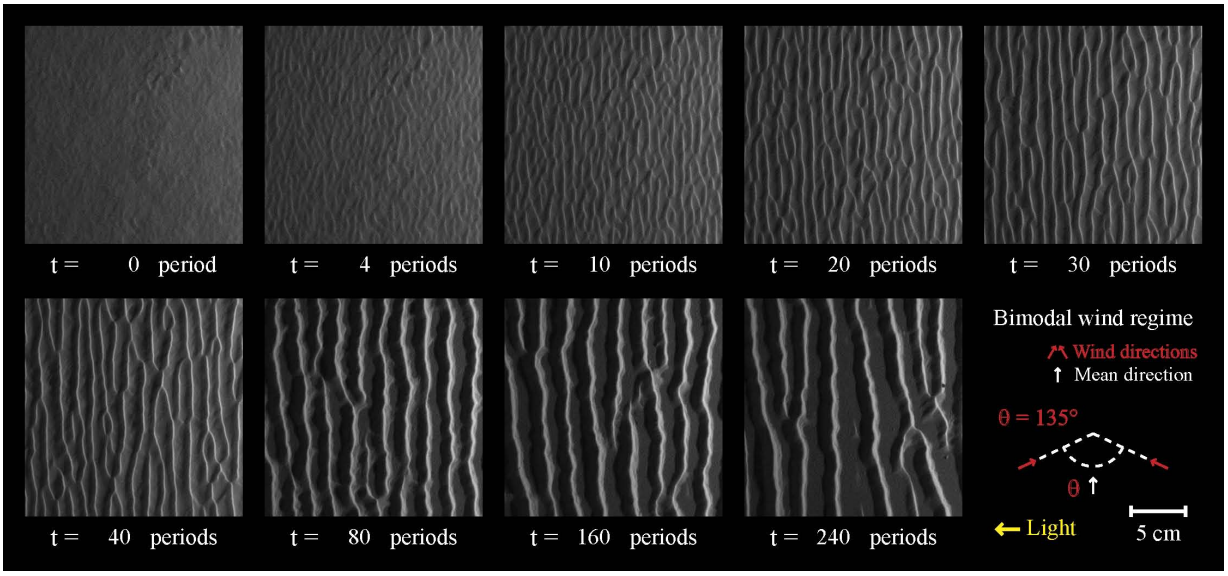

FIG. 16 **Formation of longitudinal sand dunes from a flat sand layer for** $\theta = 135°$**.** See supplementary movie *SM4* online.

D. Single transverse bar

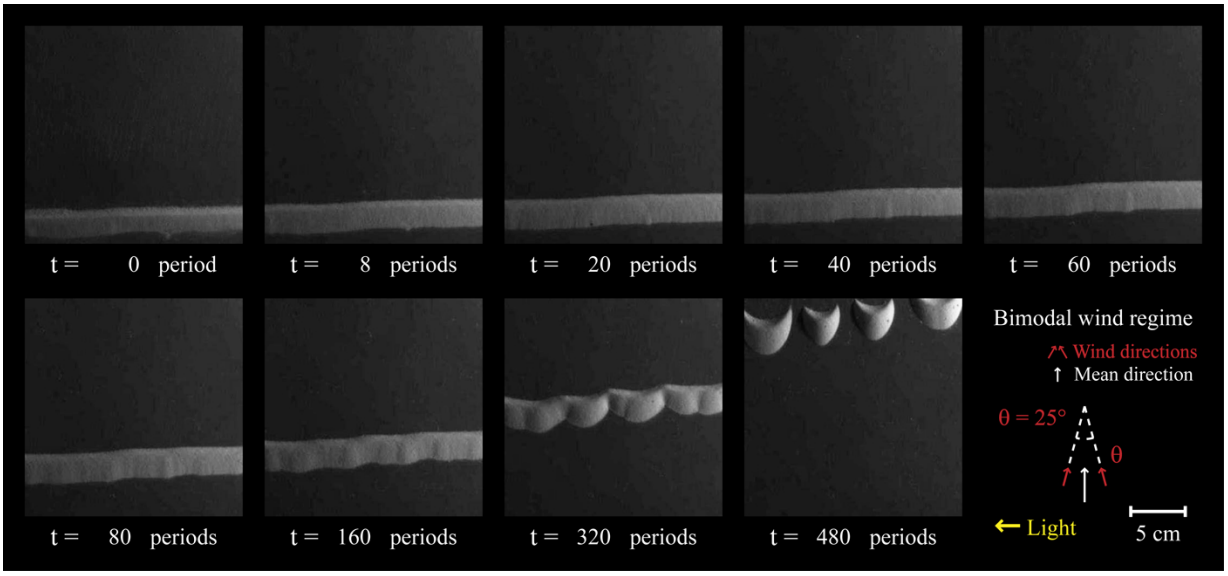

FIG. 17 **Evolution of an isolated transverse dune for $\theta = 25°$.** See supplementary movie *SM5* online.

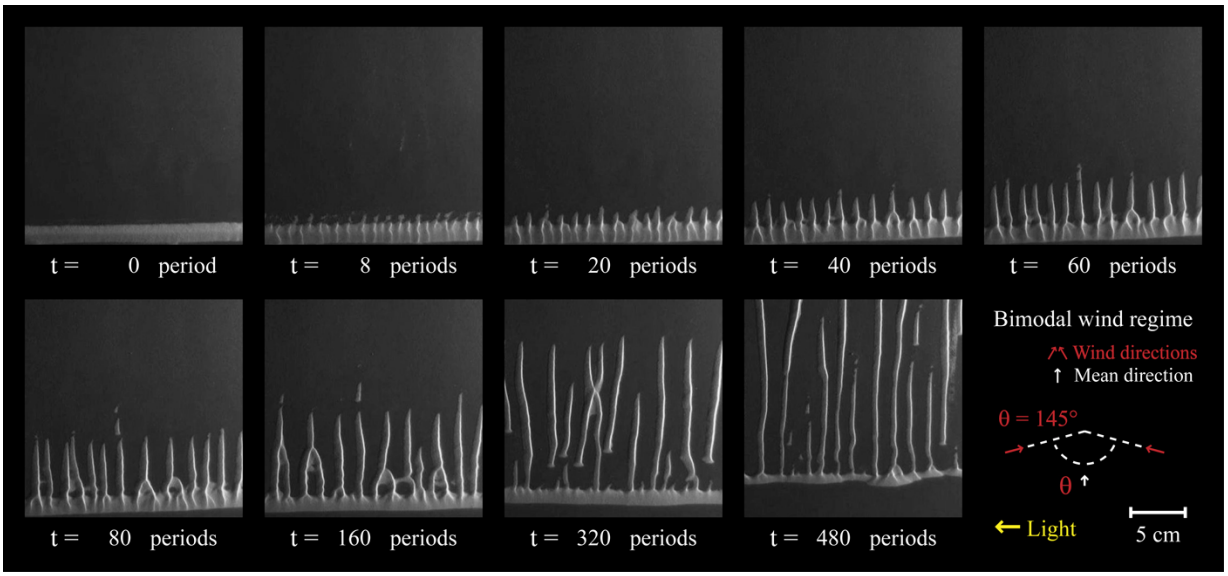

FIG. 18 **Evolution of an isolated transverse dune for $\theta = 145°$.** See supplementary movie *SM6* online.

E. Single longitudinal bar

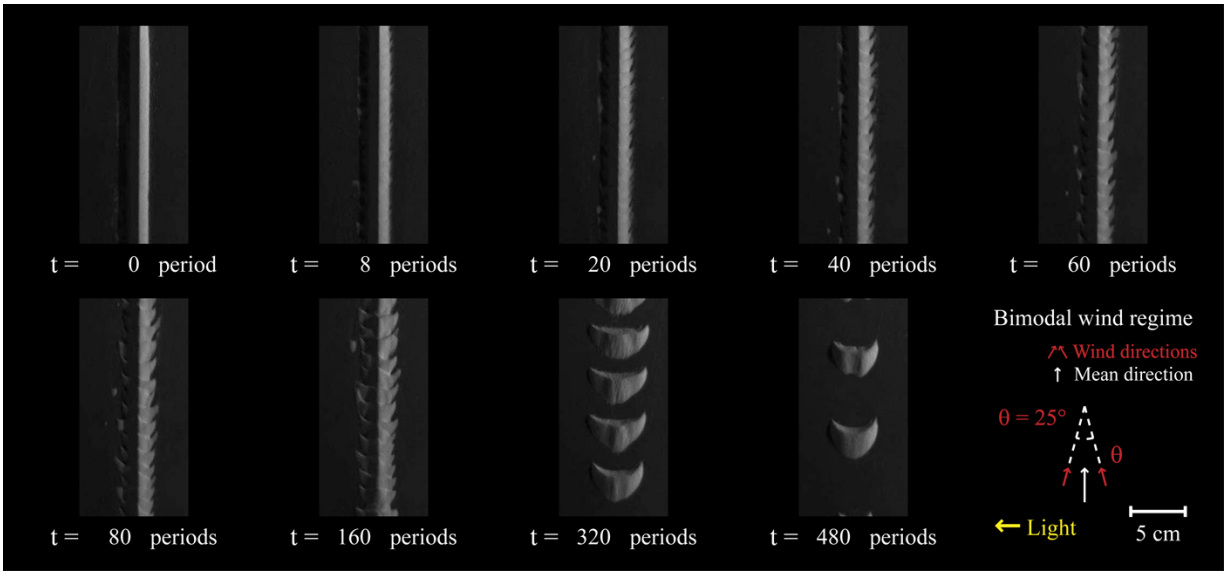

FIG. 19 **Evolution of an isolated longitudinal dune for $\theta = 25°$.** See supplementary movie *SM7* online.

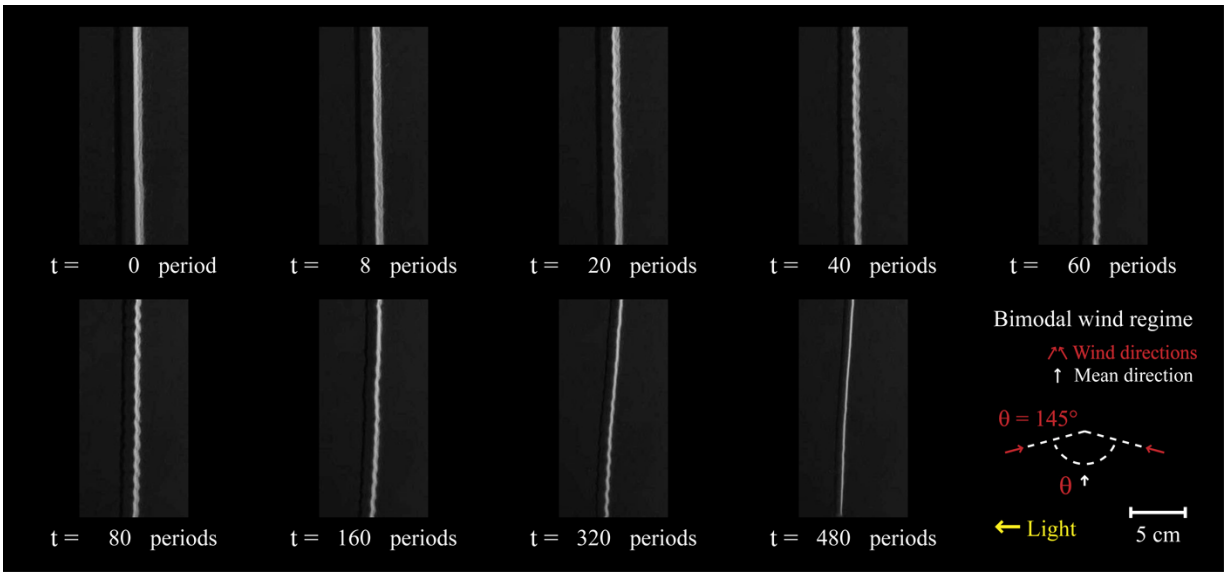

FIG. 20 **Evolution of an isolated longitudinal dune for $\theta = 145°$.** See supplementary movie *SM8* online.

F. Isolated sand patch : $\theta = 120°$

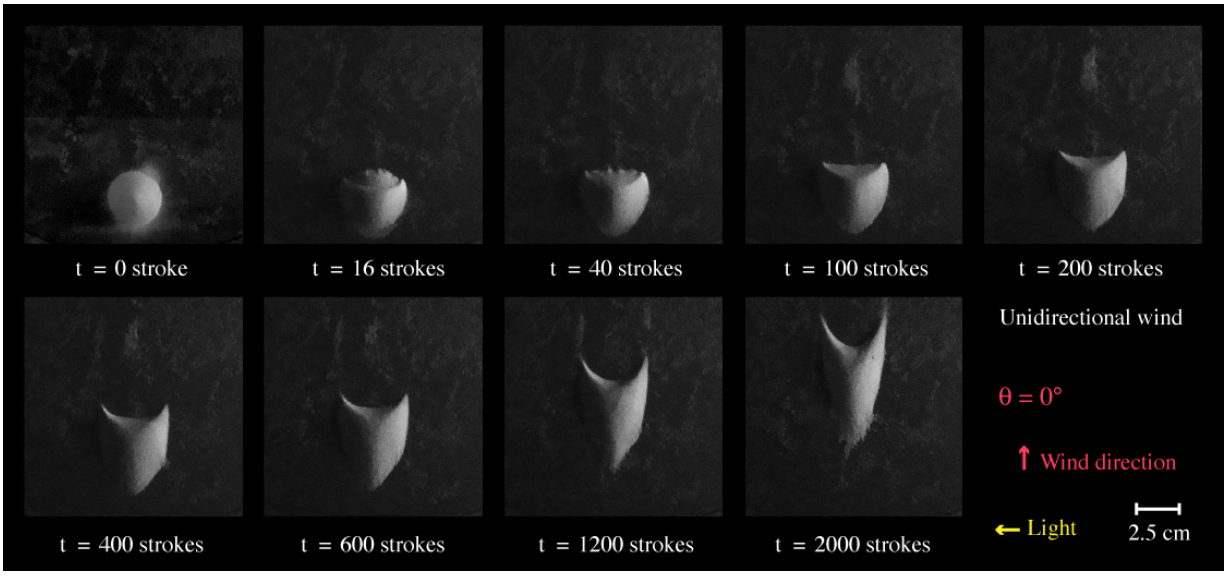

FIG. 21 **Evolution of an isolated sand patch into a** *barchan* **for** $\theta = 0°$**.** See supplementary movie *SM9* online.

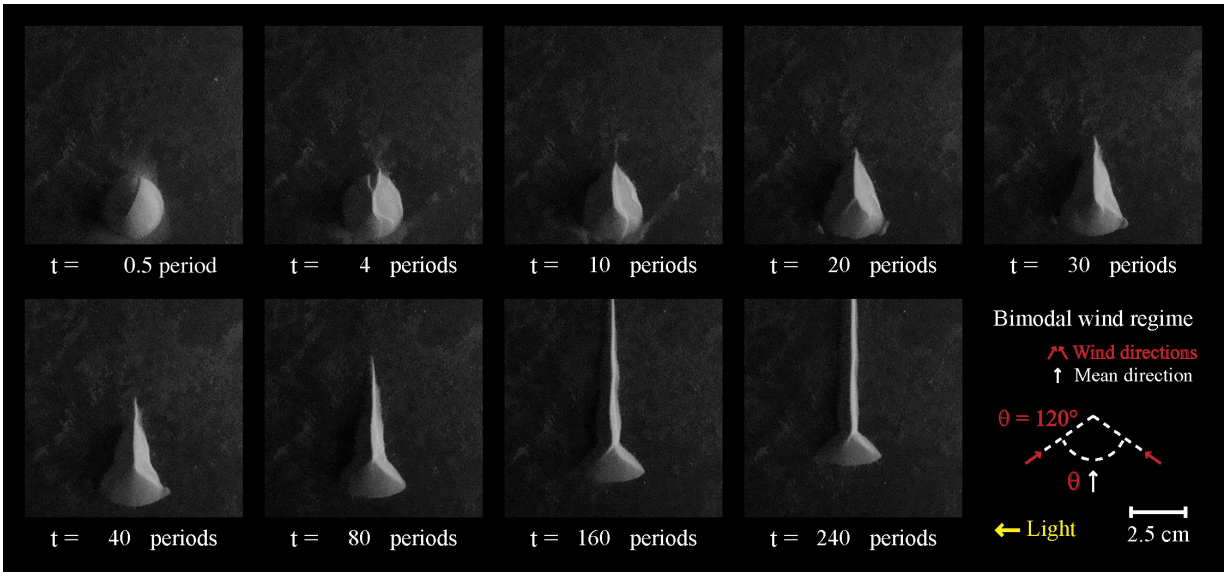

FIG. 22 **Evolution of an isolated sand patch into a longitudinal dune for** $\theta = 120°$**.** See supplementary movie *SM10* online.

References

[1] Hersen P, Douady S, Andreotti B. Relevant length scale of barchan dunes. Phys Rev Lett. **89** (26):264301 (2002).
[2] Hersen P, Douady S. Collision of barchan dunes as a mechanism of size regulation, Geophys. Res. Lett., **32**, L24103 (2005).
[3] Hersen, P. Flow effects on the morphology and dynamics of aeolian and subaqueous barchan dunes, J. Geophys. Res., **110**, F04S07 (2005).
[4] Daerr A. Dynamical equilibrium of avalanches on a rough plane, Phys. Fluids **13** (7), 2115-2124 (2001).
[5] Hersen P., Andersen K., Elbelrhiti H., Andreotti B., Claudin P., Douady S. Corridors of barchan dunes: Stability and size selection, Phys. Rev. E, **69**, 011304 (2004).
[6] K. Kroy, G. Sauermann, and H. J. Herrmann, Minimal Model for Sand Dunes, Phys. Rev. Lett. **88**, 054301 (2002).
[7] Hersen, P. On the crescentic shape of barchan dune, Eur. Phys. J. B, **37**, 507-514 (2004).
[8] Rubin, DM, Hunter, RE. Bedform alignment in directionally varying flow, Science, **237**, 276-278, (1987).
[9] Google Earth, Google Mars and Google Maps are very convenient and efficient tools to observe dunes and desert morphological features.